



Quantification of the effect of modeled lightning NO₂ on UV–visible air mass factors

Joshua L. Laughner¹ and Ronald C. Cohen^{1,2}

¹Department of Chemistry, University of California, Berkeley, Berkeley, CA 94720, USA

²Department of Earth and Planetary Sciences, University of California, Berkeley, Berkeley, CA 94720, USA

Correspondence to: Ronald C. Cohen (rccohen@berkeley.edu)

Received: 26 July 2017 – Discussion started: 4 August 2017

Revised: 4 October 2017 – Accepted: 11 October 2017 – Published: 17 November 2017

Abstract. Space-borne measurements of tropospheric nitrogen dioxide (NO₂) columns are up to 10x more sensitive to upper tropospheric (UT) NO₂ than near-surface NO₂ over low-reflectivity surfaces. Here, we quantify the effect of adding simulated lightning NO₂ to the a priori profiles for NO₂ observations from the Ozone Monitoring Instrument (OMI) using modeled NO₂ profiles from the Weather Research and Forecasting–Chemistry (WRF-Chem) model. With observed NO₂ profiles from the Deep Convective Clouds and Chemistry (DC3) aircraft campaign as observational truth, we quantify the bias in the NO₂ column that occurs when lightning NO₂ is not accounted for in the a priori profiles. Focusing on late spring and early summer in the central and eastern United States, we find that a simulation without lightning NO₂ underestimates the air mass factor (AMF) by 25 % on average for common summer OMI viewing geometry and 35 % for viewing geometries that will be encountered by geostationary satellites. Using a simulation with 500 to 665 mol NO flash⁻¹ produces good agreement with observed NO₂ profiles and reduces the bias in the AMF to < ±4 % for OMI viewing geometries. The bias is regionally dependent, with the strongest effects in the southeast United States (up to 80 %) and negligible effects in the central US. We also find that constraining WRF meteorology to a reanalysis dataset reduces lightning flash counts by a factor of 2 compared to an unconstrained run, most likely due to changes in the simulated water vapor profile.

1 Introduction

NO_x (\equiv NO + NO₂) is a short-lived (typical summer lifetime 2–7 h) trace gas in the atmosphere. NO_x is emitted by both anthropogenic and natural processes; the former is primarily due to combustion, while the latter includes biomass burning, soil bacteria nitrification or denitrification, and lightning. NO_x regulates ozone production throughout the troposphere; therefore, accurate measurements of NO_x and understanding of NO_x chemistry are essential to describe and predict the role of ozone as an air quality hazard, oxidant, and a greenhouse gas.

Space-borne measurements of NO₂ as an indicator of total NO_x, such as those from the Global Ozone Monitoring Experiment (GOME and GOME-2), SCanning Imaging Absorption SpectroMeter for Atmospheric CHartography (SCIAMACHY), and Ozone Monitoring Instrument (OMI), are a valuable tool in understanding NO_x emissions and chemistry because of their global reach and long data records. Use of these observations includes assessment of NO_x chemistry (e.g., Beirle et al., 2011; Valin et al., 2013) anthropogenic emissions (e.g., Miyazaki et al., 2012; Russell et al., 2012; Lu et al., 2015; Liu et al., 2016, 2017) and natural emissions (e.g., Martin et al., 2007; Beirle et al., 2011; Hudman et al., 2012; Mebust et al., 2011; Mebust and Cohen, 2013, 2014; Miyazaki et al., 2014; Zörner et al., 2016).

Retrieval of tropospheric NO₂ from a UV–visible satellite spectrometer requires three main steps: fitting of the measured absorbance to produce a slant column density (SCD), separation of the stratospheric and tropospheric signals, and conversion of the tropospheric SCD to a vertical column density (VCD; Boersma et al., 2011; Bucsela et al., 2013). This final step accounts for the effect of variable path length

through the atmosphere, surface elevation and reflectance, and the vertical distribution of NO_2 (Palmer et al., 2001). For observations over low-reflectivity surfaces, the sensitivity of the satellite to NO_2 decreases towards the surface, as photons penetrating into the lower atmosphere may scatter into the surface, where most are absorbed; thus, there is a higher probability that a photon that reaches the detector has interacted only with the higher levels of the atmosphere (Hudson et al., 1995; Richter and Wagner, 2011). That is to say, a given number of NO_2 molecules in the upper troposphere (UT) produce a greater signal than the same number of NO_2 molecules at the surface would. Thus, a priori knowledge of the vertical profile of NO_2 is necessary to account for this effect in the retrieval.

These vertical profiles are simulated using chemical transport models (CTMs) such as TM4 (used in Boersma et al., 2011), the Global Modeling Initiative (GMI) CTM (used in Bucselá et al., 2013), or the Weather Research and Forecasting–Chemistry model (WRF-Chem, used in Russell et al., 2011). These models must account for atmospheric transport, chemistry, emissions, and deposition to accurately simulate the required NO_2 profiles. Most of the emission of NO_2 occurs at or very near the surface. There are comparatively weaker sources of NO_2 in the upper troposphere, limited to transport from the surface, aircraft, stratospheric mixing, and lightning (Jaeglé et al., 1998).

Simulation of lightning NO_x emission in these models is typically done by assuming each flash emits a set number of molecules of NO. The number and location of lightning flashes is often parameterized using the method of Price and Rind (1992), which relates lightning flash rates to cloud top heights, which in turn are calculated from the model's meteorology. In CTMs focused on simulating surface chemistry to understand or predict air quality, such as WRF-Chem or the Community Multiscale Air Quality (CMAQ) model, including NO_x produced by lightning may be disabled by default or require the user to prepare additional input files. As these models are often used to simulate high-resolution a priori profiles (e.g., Russell et al., 2011, 2012; Kuhlmann et al., 2015; Laughner et al., 2016; Goldberg et al., 2017), the absence of lightning NO_x from the a priori profiles may contribute to a significant bias in the interpretation of the measurements (e.g., Travis et al., 2016).

In the upper troposphere, NO_x lifetime has previously been assumed to be long (2–8 days, Schumann and Huntrieser, 2007). Recently, work from the Deep Convective Clouds and Chemistry (DC3) campaign showed that the lifetime of NO_x is short near thunderstorms due to active alkyl-, peroxy-, and multifunctional-nitrate chemistry with peroxy radicals formed in the near field from organic precursors lofted from the boundary layer (~ 3 h, Nault et al., 2016) but longer (12–48 h, Nault et al., 2016) away from thunderstorms once these radical species are consumed and other controlling factors take over (Bertram et al., 2007; Apel et al., 2012). In either case, lightning NO_x can affect upper tropo-

spheric NO_x concentrations distant from active storms; thus, simulated lightning NO_x will have wide-reaching and persistent effects on a priori NO_2 profiles throughout a model domain. Previous work by, for example, Beirle et al. (2009) and Pickering et al. (2016) has provided careful analysis of the effect of lightning on AMFs (air mass factors) in the near field of a thunderstorm, with the goal of improving direct satellite measurements of the mean production of NO per flash. Goldberg et al. (2017) compared high-resolution NO_2 profiles from the Community Multiscale Air Quality model with those from a lower-resolution GMI model and found that the CMAQ profiles had less upper troposphere NO_2 than the GMI profiles, despite greater lightning emissions in CMAQ. Our goal here is to consider the broader impact of modeled lightning NO_x on satellite retrievals on the full domain both near and far from the lightning event.

In this work, we evaluate the impact of modeled lightning NO_x on NO_2 a priori profiles simulated with the WRF-Chem chemical transport model for a domain covering the central and eastern US. We first consider the problem in a general sense, with a sensitivity test using three profiles simulated with different amounts of lightning NO_x . We then compare modeled profiles to observations from the DC3 campaign to determine the accuracy of AMFs derived using the simulated profiles and finally implement these profiles in an NO_2 retrieval to demonstrate the spatial pattern and significance of this effect in a real application.

2 Methods

2.1 The Deep Convective Clouds and Chemistry campaign

The Deep Convection Clouds and Chemistry (DC3) campaign is an aircraft measurement campaign that took place between 18 May and 22 June 2012 throughout the central and southeastern US (Barth et al., 2015). The NASA DC-8 aircraft sampled outflow from convective systems, studying direct and aged lightning NO_x emissions. We use NO_2 measurements made by laser-induced fluorescence at 1 s resolution in this study (Thornton et al., 2000; Nault et al., 2015).

2.2 Weather Research and Forecasting–Chemistry model

We use the Weather Research and Forecasting–Chemistry model v. 3.5.1 (Grell et al., 2005) to simulate NO_2 profiles across a domain that covers the same region as the DC3 campaign at 12 km model resolution with 29 vertical levels. Meteorological initial and boundary conditions are driven by the North American Regional Reanalysis (NARR) dataset. Chemical initial and boundary conditions are driven by output from the Model for Ozone and Related Chemical Tracers (MOZART; Emmons et al., 2010) provided by the National Center for Atmospheric Research (NCAR). An-

thropogenic emissions are driven by the National Emissions Inventory 2011 (NEI 11); each emitted species is scaled domain wide by the ratio of its total annual 2012 to 2011 emissions provided by the Environmental Protection Agency (EPA, 2016); e.g., 2012 NO_x emissions are given at 13.657 million t, which is 94 % of the 2011 value of 14.519 million t; the gridded 2011 NO emissions are multiplied by 0.94 to obtain the 2012 emissions. Biogenic emissions are driven by the Model of Emissions of Gases and Aerosol from Nature (MEGAN; Guenther et al., 2006). The chemical mechanism is a customized version of the Regional Atmospheric Chemistry Mechanism, version 2 (RACM2; Goliff et al., 2013) that includes updates to alkyl nitrate chemistry from Browne et al. (2014) and Schwantes et al. (2015), as well as formation, dissociation, and photolysis of methyl peroxy nitrate (MPN; Browne et al., 2011, see also http://wiki.seas.harvard.edu/geos-chem/images/GEOS_changes_MPN_chemistry.pdf) Instantaneous values of the model output are sampled every 30 min.

WRF can be run such that the meteorology within the domain is driven by the model physics chosen, constrained by reanalysis meteorology data only through the initial and boundary conditions. Alternatively, four-dimensional data analysis (FDDA) nudging (Liu et al., 2005; Stauffer and Seaman, 1990; Stauffer et al., 1991) can be used to nudge the model meteorology towards a reanalysis meteorology product throughout the domain. We use this capability in two WRF-Chem simulations, nudging towards the NARR meteorology. In all other simulations, the meteorology evolves according to the model physics.

Lightning NO_x emissions are calculated by the standard modules in WRF-Chem 3.5.1, with a slight modification to the assumed emission profile (described below). The flash rates (number of lightning flashes per unit time) are determined by the Price and Rind level of neutral buoyancy parameterization (Price and Rind, 1992), which depends on cloud top height, calculated using the Grell 3D cumulus physics (Grell, 1993; Grell and Dévényi, 2002) with Lin microphysics (Lin et al., 1983). This number of flashes calculated may be scaled by a constant factor, we use this functionality for one run in Sect. 3.2, otherwise the scaling factor is 1. The intra-cloud/cloud-to-ground ratio is prescribed using the Boccippio et al. (2001) climatology; both intra-cloud and cloud-to-ground flashes are specified to generate the same number of moles of NO per flash (Cooray et al., 2009; Ott et al., 2010), which for this study is 0, 500, or 665 mol flash⁻¹. These values are chosen to represent no lightning, the standard midlatitude assumption (500 mol flash⁻¹ Hudman et al., 2007), and the recently proposed 33 % increase in lightning NO_x emissions of Nault et al. (2017) (665 mol flash⁻¹).

The vertical distribution of NO emissions is driven by a modified version of the profiles from Ott et al. (2010). Several recent studies (Allen et al., 2012; Seltzer et al., 2015) suggest that the standard Ott profiles place too much NO_x in

the mid-troposphere. Ott et al. (2010) calculated these profiles using a polynomial fit to profiles of the post-convection vertical distribution of lightning NO_x simulated by a cloud-resolving model. The midlatitude profile generated by the cloud-resolving model has a bimodal distribution not captured by the polynomial fit; therefore, we replace the standard (polynomial fit) Ott et al. (2010) midlatitude profile in WRF-Chem with the bimodal profile.

2.3 Matching aircraft and model data

We match WRF-Chem data to DC3 observations to evaluate the accuracy of the chosen lightning parameterization. Each 1 s DC3 NO_2 observation is paired with the corresponding WRF-Chem data point. Data points are matched in time by finding the WRF-Chem output file (available every 30 min) nearest in time to a given DC3 observation.

Horizontally, a WRF-Chem data point is said to match with a DC3 observation if the latitude and longitude of the DC3 observation lie within the box defined by the midpoints of the WRF-Chem grid cell edges. These midpoints are computed as the average of the relevant corner coordinates (e.g., the western edge point is the average of the northwestern and southwestern corners); the corner coordinates are calculated by assuming that corners not on the edge of the domain are the average of the four surrounding centers. Corners on the domain edge are calculated by extrapolating from the internal corners.

Vertically, we find the matching WRF-Chem data point from the column of such points identified by the previous two steps by finding the WRF-Chem grid point with the smallest difference in pressure compared to the DC3 observation. The result is two vectors of NO_2 concentrations (DC3 and WRF-Chem) that are the same length; WRF-Chem data points that correspond to multiple DC3 observations are repeated, thus inherently giving them more weight and reflecting the sampling of the aircraft. Matching the vertical position in this way inherently restricts the model data to the vertical range of the observations.

2.4 The Ozone Monitoring Instrument

The Ozone Monitoring Instrument is a polar-orbiting, nadir-viewing UV-visible spectrometer onboard the Aura satellite, launched in 2004. It has a nadir pixel size of $13 \times 24 \text{ km}^2$. The primary detector is a 2D charge-coupled device array that observes a swath width of 2600 km and a spectral range of 270–500 nm (Levelt et al., 2006). It provides daily global observation for the first 3 years of operation; after 2007 several detector rows developed anomalous radiances (termed the “row anomaly”, <http://projects.knmi.nl/omi/research/product/rowanomaly-background.php>) that have expanded over time; from July 2011 on, this affects approximately one-third of the pixels. There are two publicly available global products of NO_2 column densities,

the KNMI DOMINO product (Boersma et al., 2011) and the NASA standard product v3 (Krotkov et al., 2017), and numerous regional products, including OMI-EC (McLinden et al., 2014), Hong Kong OMI NO₂ (Kuhlmann et al., 2015), Peking University OMI NO₂ (POMINO Lin et al., 2015), Empa OMI NO₂ (EOMINO, <http://temis.empa.ch/index.php>), DOMINO2_GC (Vinken et al., 2014), and the Berkeley High-Resolution OMI NO₂ retrieval (Russell et al., 2011, 2012).

2.5 Berkeley High-Resolution OMI NO₂ retrieval

2.5.1 Retrieval product

To demonstrate the impact of modeled lightning NO_x on retrieved NO₂ column densities, we use v2.1C of the Berkeley High-Resolution (BEHR) NO₂ retrieval. Details of the algorithm are given in Russell et al. (2011); more recent updates are given in the changelog (<http://behr.cchem.berkeley.edu/Portals/2/Changelog.txt>). This product is available for download at <http://behr.cchem.berkeley.edu/DownloadBEHRData.aspx>.

Version 2.1C of the BEHR product is based on the NASA standard product version 2 (SP v2). It uses the OMI total slant column densities from the OMI NO₂ product OMNO2A v1.2.3 (Boersma et al., 2002; Bucsela et al., 2006, 2013), as well as the stratospheric separation and destripping from the NASA standard product v2. Version 3 of the NASA standard product was released in 2016 and includes new spectral fitting and tropospheric AMF calculations. The change from SP v2 to v3 does not affect any of the AMF calculations in this work. Krotkov et al. (2017) indicates that the tropospheric vertical column densities over unpolluted areas are similar between SP v2 and v3; therefore, when effects on retrieved VCDs are considered here, we expect our conclusions to be unaltered when BEHR is updated to use SP v3 data.

The BEHR product recalculates the tropospheric air mass factor using the formulation in Palmer et al. (2001). In previous versions of BEHR, the tropospheric AMFs and resulting vertical column densities were always “total” tropospheric columns; i.e., they included an estimated ghost NO₂ column below clouds. The ghost column was estimated by using as the AMF the ratio of the visible modeled slant column (derived from the a priori NO₂ profile, scattering weights, and radiance cloud fraction) to the total modeled tropospheric vertical column. Thus, dividing the observed slant column by this AMF produced a total tropospheric vertical column via a multiplicative correction. This approach is identical to that described in Boersma et al. (2002).

Starting in v2.1C, “visible-only” tropospheric AMFs and VCDs are included (which do not include the below-cloud ghost column), in addition to the “total” tropospheric VCDs. In both cases, separate AMFs for clear and cloudy scenes are

calculated using Eq. (1).

$$\text{AMF} = \int_{p_0}^{p_{\text{tp}}} w(p)S(p) dp, \quad (1)$$

where p_0 is the surface or cloud pressure (for clear and cloudy scenes, respectively), p_{tp} is the tropopause pressure (fixed at 200 hPa), and $w(p)$ is the vector of the pressure-dependent scattering weights from the TOMRAD lookup table used in the NASA SP v2 (Bucsela et al., 2013), which must be corrected for the temperature dependence of the NO₂ cross section:

$$w(p) = w_0(p) [1 - 0.003(T(p) - 220)], \quad (2)$$

where $w_0(p)$ is the scattering weight from the lookup table and T is the temperature in Kelvin for a given latitude, longitude, and month; T is taken from the same temperature profiles used in the NASA SP v2 (Bucsela et al., 2013). Recently, an error in the temperature profile lookup for BEHR v2.1C was identified. This caused a $\sim 5\%$ bias in the AMFs, but it has been corrected for this study.

Finally, $S(p)$, the shape factor, is computed as

$$S(p) = \left(\int_{p_s}^{p_{\text{tp}}} g(p) dp \right)^{-1} g(p), \quad (3)$$

where $g(p)$ is the NO₂ vertical profile, and p_s is either the surface or cloud pressure, depending on whether a total (visible + ghost) or visible-only tropospheric VCD is desired. BEHR v2.1C provides both total and visible-only tropospheric VCDs. For clear scenes, p_s is always the surface pressure. For cloudy scenes, p_s is the surface pressure when calculating the total tropospheric VCD and the cloud pressure when calculating the visible-only VCD.

The clear and cloudy AMFs for a given pixel are combined as

$$\text{AMF}_{\text{trop}} = (1 - f)\text{AMF}_{\text{clear}} + f\text{AMF}_{\text{cloudy}}, \quad (4)$$

where f is the radiance cloud fraction, i.e., the fraction of light from the pixel that is reflected off of clouds. The final VCD is computed as

$$\text{VCD} = \frac{\text{SCD}}{\text{AMF}_{\text{trop}}}, \quad (5)$$

where the SCD is the tropospheric slant column density from the NASA SP v2.

The vector of scattering weights, $w(p)$, chosen from the TOMRAD lookup table depends on five parameters: solar zenith angle (SZA), viewing zenith angle (VZA), relative azimuth angle (RAA), albedo, and surface pressure. The SZA, VZA, and RAA are directly provided or can be calculated

Table 1. The values used for the five input parameters to the AMF TOMRAD lookup table in the sensitivity tests. Albedo (Alb) and surface pressure have different sets of values when the sensitivity test is looking at clear sky and cloudy sky scenarios. For cloudy scenes, the cloud pressure (Cld P) is used as the surface pressure (Surf P).

Parameter	Abbreviation	Values	Unit
Solar zenith angle	SZA	0, 11, 22, 33, 44, 55, 66, 77, 88	degree
Viewing zenith angle	VZA	0, 14, 28, 42, 56, 70	degree
Relative azimuth angle	RAA	0, 45, 90, 135, 180	degree
Albedo (clear sky)	Alb	0, 0.009, 0.018, 0.027, 0.036, 0.044, 0.053, 0.062, 0.071, 0.080	unitless
Albedo (cloudy sky)	Alb	0.700, 0.722, 0.744, 0.767, 0.789, 0.811, 0.833, 0.856, 0.878, 0.900	unitless
Surface pressure (clear)	Surf P	1013, 989, 965, 940, 916, 892, 868, 843, 819, 795	hPa
Cloud pressure (cloudy)	Cld P	1003, 930, 857, 783, 710, 637, 564, 490, 417, 344	hPa

from data provided in the NASA SP v2. The surface albedo for a given pixel is calculated by averaging the black sky albedo product MCD43C3 (Schaaf and Wang, 2015) values that fall within the pixel. This product is generated by the Moderate Resolution Imaging Spectroradiometer (MODIS) instruments onboard the Aqua and Terra satellites. Clouds are assumed to have an albedo of 0.8 (Stammes et al., 2008). Surface pressures are calculated by averaging elevation data from the Global Land One-km Base Elevation project (Hastings and Dunbar, 1999) that falls within the pixel and assuming a scale height of 7.4 km; cloud pressures are from the OMI O₂–O₂ algorithm (Acarreta et al., 2004; Sneep et al., 2008; Bucselo et al., 2013) and are included in the NASA SP v2.

When averaging over time for the results in Sect. 3.3 we only use pixels with the OMI geometric cloud fraction < 0.2, XTrackQualityFlags = 0, and an even integer for VcdQualityFlags. The averages weight each pixel's contribution by the inverse of the pixel area. Unless otherwise stated, all results in this work use the total tropospheric column.

2.5.2 AMF sensitivity tests

To understand the sensitivity of the AMF to the profile shape under different conditions, we carry out sensitivity tests by varying the five input parameters to the TOMRAD lookup table. Table 1 lists the input parameters and the values used for each parameter. For albedo and surface pressure, two sets of values are used; one represents common values seen for clear (unclouded) scenes and the other for cloudy scenes. In cloudy scenes, the cloud pressure is used as the surface pressure. The range of values for SZA, VZA, and RAA span the values defined in the TOMRAD lookup table. The range of values for albedo (clear sky), surface pressure (clear sky), and cloud pressure (cloudy) span the average 5th and 95th percentiles of those values observed in 7 days of BEHR data (1 to 7 June 2012). The limits for albedo (cloudy) are chosen as 0.8 ± 0.1 , i.e., the assumed cloud albedo plus a reasonable range to explore.

Scattering weights are calculated for every combination of clear or cloudy parameters (27 000 combinations). We

choose the temperature correction (Sect. 2.5.1, Eq. 2) assuming the June temperature profile at 37.5° N, 95° W. Using a single NO₂ profile, an AMF is calculated for every combination of input parameters.

We use three types of NO₂ vertical profiles for the AMF sensitivity tests.

1. One derived from the 1 s DC3 NO₂ data (Sect. 2.1)
2. One using WRF-Chem output matched to the DC3 flight path (Sect. 2.3)
3. One using WRF-Chem output averaged over the entire domain between 17:00 and 22:00 UTC (roughly the times during which OMI is over North America)

In all cases the data points (modeled or measured) used to generate the NO₂ profiles are binned by pressure to generate a profile defined at the same pressures (using pressure as a vertical coordinate) as the scattering weights in the lookup table. Each data point is placed in the bin with the scattering weight pressure closest to the pressure of the data point. When using the DC3–WRF matched profiles (Sect. 2.3), the two greatest surface pressures (1013 and 989) would have essentially no difference, as the matched profiles only extend down to 990 hPa.

3 Results

3.1 Parameter sensitivity study using modeled profiles

We begin by demonstrating the sensitivity of the AMF to modeled lightning NO_x emissions in a general sense. Profiles used in this section are those derived by binning WRF-Chem output from the entire domain for simulations with 0, 500, and 665 mol NO flash⁻¹ without FDDA nudging (Fig. 1). Figure 2 shows the percent difference in the AMF when using the profile simulated with 500 mol NO flash⁻¹ versus 0 mol NO flash⁻¹. In each plot, two of the lookup table inputs are varied and two are held constant. Each plot represents the change averaged over all values of relative azimuth

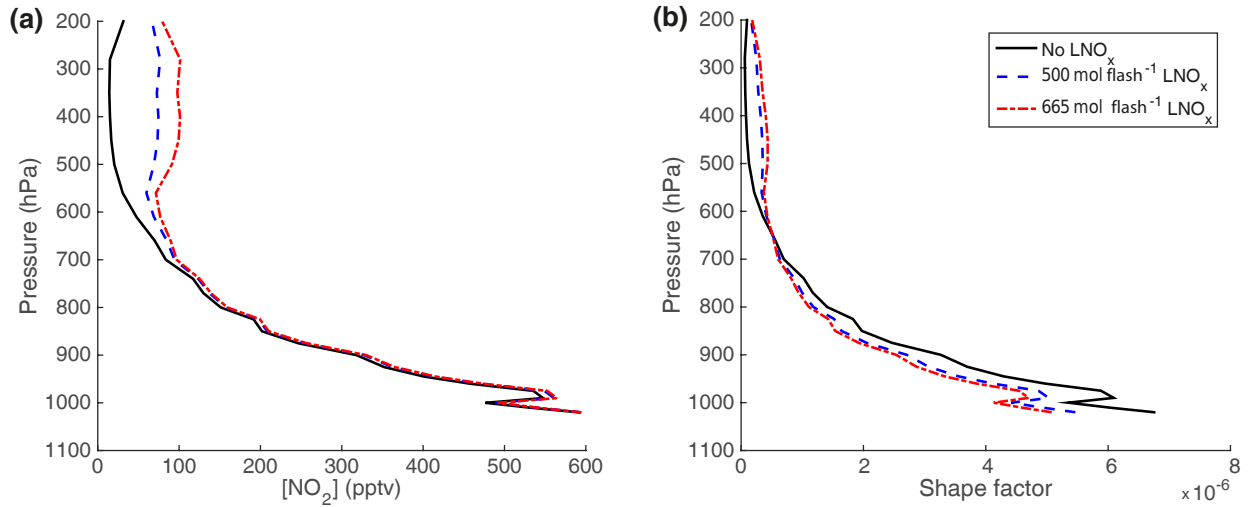


Figure 1. Domain-wide mean WRF-Chem NO_2 profiles. (a) Profiles in mixing ratios; (b) profiles in shape factor as defined in Palmer et al. (2001), i.e., number density divided by VCD. LNO_x is lightning NO_x .

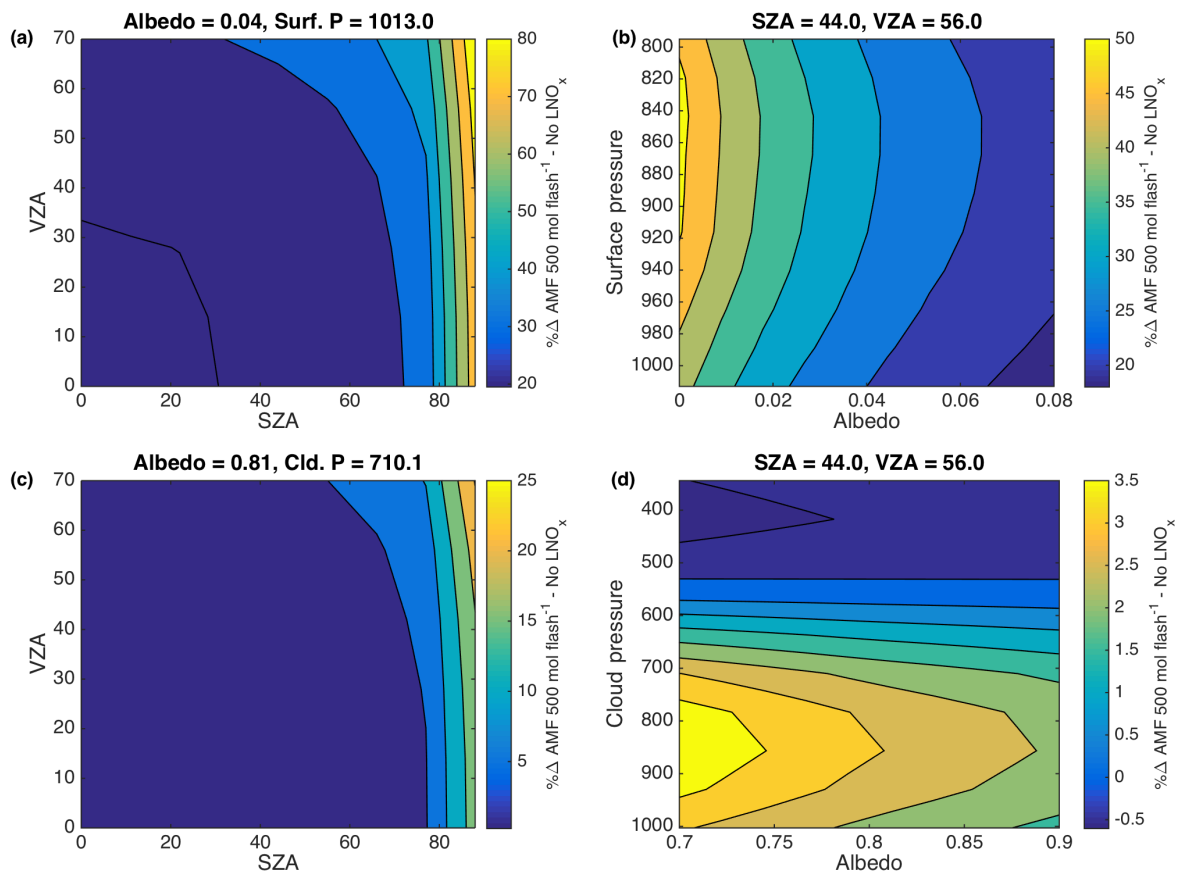


Figure 2. Contour plots of the percent change in the AMF when changing from the mean profile without lightning NO_x to the mean with lightning NO_x ($500 \text{ mol flash}^{-1}$), averaged over the whole WRF-Chem domain. The differences are averaged over all values of RAA. In each plot, two parameters are varied while the other two are held constant. The values of the constant parameters are given above each plot. Panels (a) and (b) use a range of albedos and surface pressure representative of clear pixels; panels (c) and (d) use a range of albedos and cloud pressure representative of cloudy pixels.

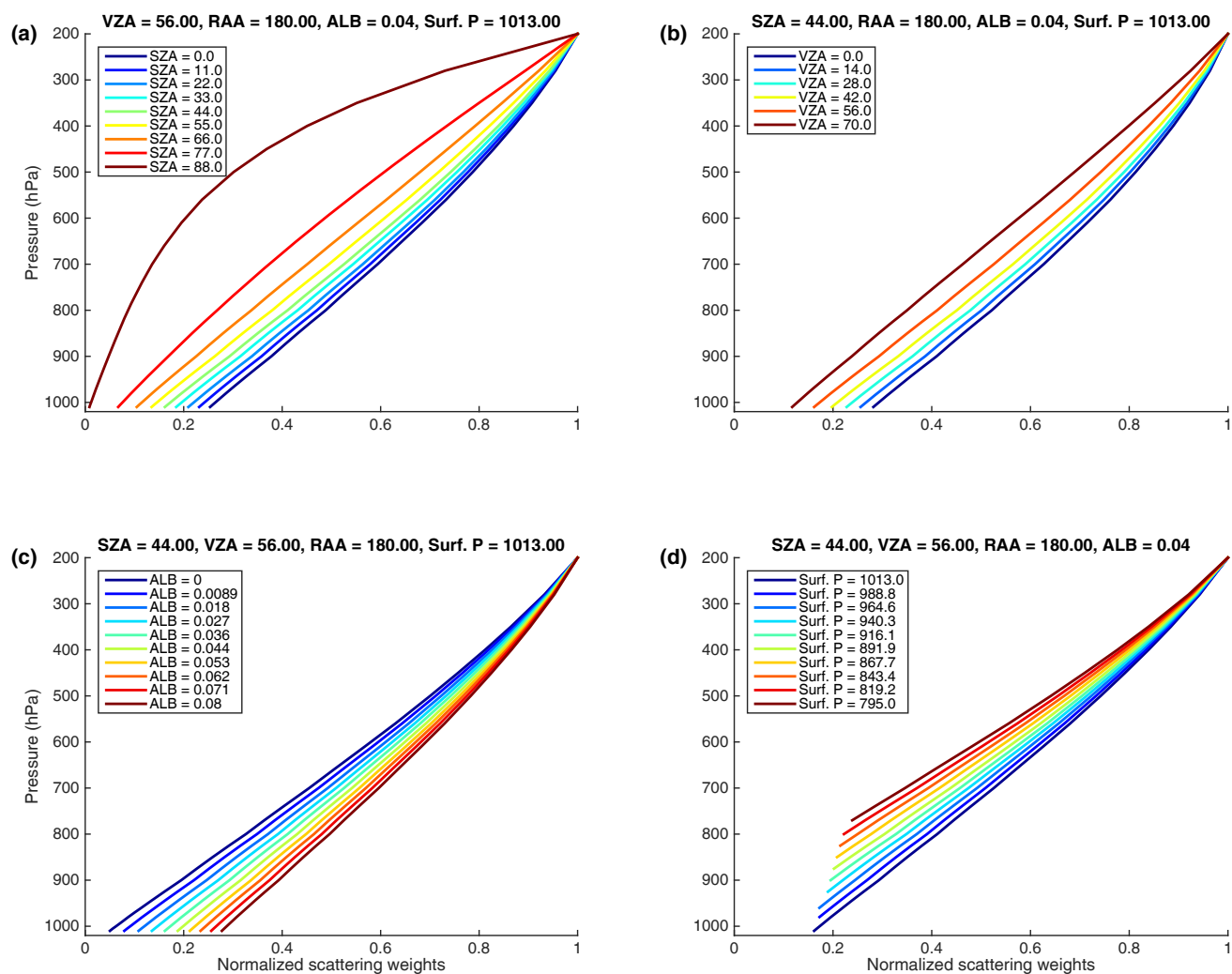


Figure 3. Vectors of scattering weights and their variation with each of the four most important lookup table input parameters. Values are representative of clear sky conditions. Each scattering weight vector is scaled so that the topmost entry is 1. Scattering weights are only shown above the surface pressure.

angle, since RAA has a small impact on the AMF (Fig. S1 in the Supplement).

Under both clear and cloudy conditions, the largest differences in AMF between the two profiles are seen at large SZAs (Fig. 2a and c). This reflects the longer average optical path through the upper troposphere at larger SZAs, causing greater sensitivity to UT NO_2 . A similar, though smaller, effect is also seen for larger VZAs.

If viewing geometry is held constant and albedo and surface pressure varied, the largest sensitivity of the AMF to simulated lightning NO_x can be seen at very low albedo and moderate surface pressure (~ 860 hPa) for clear conditions (Fig. 2b). The cause for this is illustrated in Fig. 3; Fig. 3c shows how the scattering weight vectors change with albedo and Fig. 3d shows how they change with surface pressure. Lower albedos yield lower sensitivity to near-surface

NO_2 (note that scattering weights are proportional to sensitivity) because a photon that reaches the near-surface NO_2 will likely be absorbed if it scatters into the surface (Hönniger et al., 2004). The 500 mol flash $^{-1}$ profile does have more NO_2 in the boundary layer than the no-lightning profile, especially below 900 hPa. This partly balances the increase in UT NO_2 from lightning, as there are increases at both low- and high-sensitivity altitudes. As surface pressure decreases (i.e., higher in elevation), the altitude of minimum sensitivity moves up. The surface integration limit for Eqs. (1) and (3) reduces as well, removing part of the boundary layer profile. Taken together, these changes put more weight on the UT profile and remove the > 900 hPa increase that counteracts part of the change in the UT (thus increasing the impact of lightning NO_x) until ~ 860 hPa. At ~ 860 hPa, most of the boundary layer is no longer included in the AMF calcula-

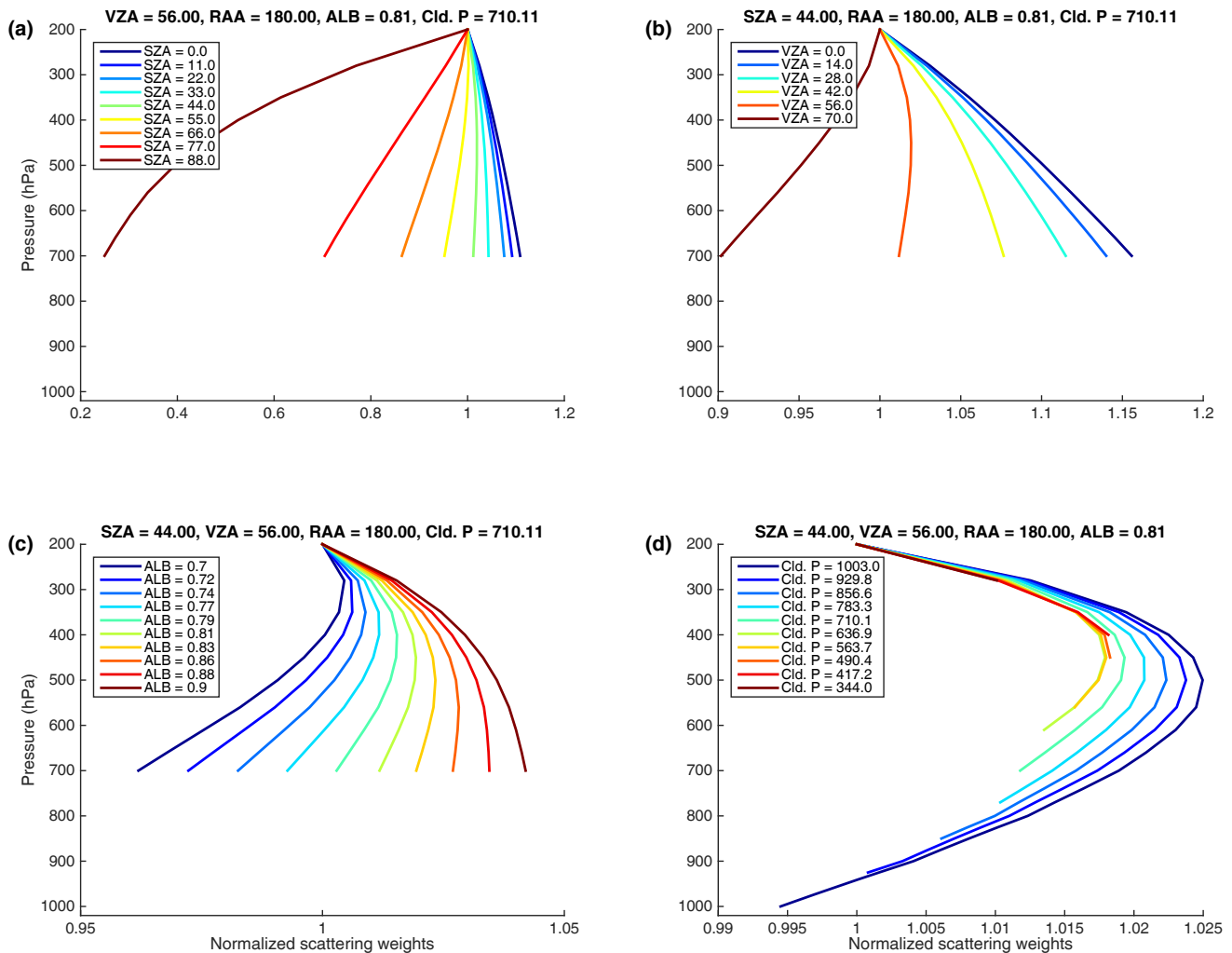


Figure 4. As in Fig. 3, but for cloudy conditions. Note that the x axis limits are different from Fig. 3 and each other.

tion. Figure 1 shows that above ~ 800 hPa the WRF-Chem profiles start to diverge due to the different amounts of lightning NO_x in each simulation. Therefore, as surface pressure moves above 850–800 hPa, the sensitivity to lightning NO_x begins to decrease because the entire extent of the profile that is integrated changes with changes in the simulated lightning NO_x . Since the profile is normalized to the column amount (Eq. 3), only the relative distribution of NO_2 matters, and the relative distribution changes very little with the magnitude of lightning NO_x emitted when only considering the part of the profile influenced by lightning NO_x .

The effect of changing surface pressure in a regular retrieval will likely be different than that described above, because the above analysis assumes that the profile does not change with surface pressure, where in fact it should, since surface-based emissions will move up with the surface. Consequently, the boundary layer maximum would not be cut off in that case. The effect described here is more consistent (i) with the effect of clouds or an aerosol layer that creates an

effectively higher altitude surface (due to scattering) or (ii) if using coarse enough a priori profiles that the surface pressure of a pixel is significantly different than the surface pressure in the model used to simulate the profile.

Cloudy conditions exhibit less sensitivity than clear conditions to the amount of lightning NO_x in the modeled profiles due to this shielding effect: in many cases, the cloud is at a sufficiently high elevation to obscure the part of the NO_2 profile influenced by surface emissions and therefore restricts the profile to the component influenced by lightning NO_x . As previously discussed with respect to surface pressure, this means that the relative distribution of NO_2 in the visible component of the profile does not change significantly. This is apparent in Fig. 2, where panels (c) and (d) show responses roughly one-fourth and one-tenth of the magnitude, respectively, compared to panels (a) and (b).

Cloudy conditions also tend to have more uniform scattering weights (Fig. 4) due in large part to their high albedo. At high albedo, the probability of “losing” photons to absorp-

tion at the surface is significantly reduced, so the reduction in sensitivity towards the surface found with low albedos does not occur. At sufficiently high albedos, there is an enhancement in sensitivity near the cloud due to the possibility of extended optical paths near the surface from multiple scattering (Richter and Wagner, 2011).

From Fig. 4, it is clear why the impact of lightning NO_x is small in Fig. 2d. For all but the most extreme sun-satellite geometries, the scattering weights are fairly uniform across all altitudes; thus, the impact of changes to the relative distribution of NO_2 within the UT is minimized since a UV-visible satellite instrument is similarly sensitive to NO_2 at any altitude under these conditions. At larger SZAs and VZAs, the cloudy scattering weights do decrease towards the cloud because Rayleigh scattering has a greater effect on the transmitted light along the longer beam paths, scattering photons at higher altitudes and so reducing the fraction of photons observed by the satellite that penetrate to the cloud (Richter and Wagner, 2011). However, the impact is less than in clear conditions. From Fig. 2c, at the largest SZA and VZA simulated, the difference in AMF between the no-lightning and 500 mol flash $^{-1}$ profiles is +20–25 % – large, but only one-fourth that of clear conditions.

The difference in the AMF obtained using profiles with 665 and 500 mol NO flash $^{-1}$ follows essentially the same pattern as shown in Figs. 3 and 4, but with one-tenth to one-fifth the magnitude (Fig. S2). The only difference in the shape of the contours is that the maximum difference occurs at greater (i.e., lower altitude) surface pressures, because the 665 and 500 mol flash $^{-1}$ profiles are mostly identical in the boundary layer, so the slight countervailing increase in boundary layer NO_2 between the 0 and 500 mol flash $^{-1}$ profiles that offset part of the UT increase is not present.

3.2 Comparison with observed profiles

Given the large sensitivity of AMFs to the presence of lightning NO_x in the a priori profiles, it is necessary to use a priori profiles that are consistent with observations. Figure 5 compares the average NO_2 profile measured in the DC3 campaign (Sect. 2.1) with WRF-Chem profiles averaged along the DC3 flights (Sect. 2.3) for five simulations. It is immediately apparent that the WRF-Chem simulation with no lightning is missing a significant amount of UT NO_2 compared to the observed DC3 profile. Both unnudged WRF-Chem simulations with lightning NO_x enabled do qualitatively capture this UT NO_2 ; however, the vertical distribution is biased compared to the DC3 observations with a maximum at 500 hPa not seen in the observed profile and less NO_2 between 300–200 hPa than in the observed profile.

We consider how significant these differences between the simulated and observed profiles are in the context of the AMF calculation. To focus only on the effect of the UT profile, we use hybrid profiles. The hybrid profiles for the unnudged 500 mol flash $^{-1}$ are illustrated in Fig. 5b. The

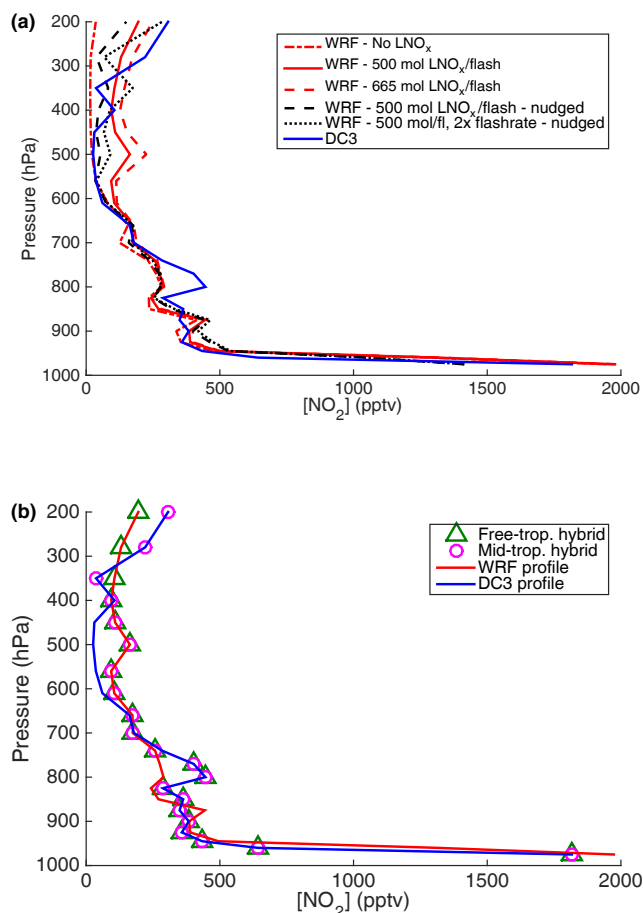


Figure 5. (a) Comparison of the NO_2 profiles obtained from binning all DC3 data and WRF-Chem output along the DC3 flight track (Sect. 2.3) to pressure bins centered on the pressure the scattering weights are defined at. (b) The binned DC3 and WRF-Chem (500 mol flash $^{-1}$, no nudging) profiles; green triangles mark pressure levels from each profile used in the free-troposphere hybrid profile, and magenta circles mark pressure levels used in the mid-troposphere hybrid profile.

free-troposphere hybrid uses the DC3 profile up to 750 hPa and the WRF-Chem profile above that, while the mid-troposphere hybrid only uses the WRF-Chem profile between 750 and 375 hPa. The free-tropospheric hybrid profile focuses on the effect of lightning NO_2 on the AMF by removing the difference in the boundary layer between the WRF-Chem and DC3 profiles, while the mid-troposphere hybrid similarly focuses on the effect of the local NO_2 maximum around 500 hPa that is not present in the DC3 profile.

Table 2 gives the results of AMF sensitivity tests (Sect. 2.5.2) on various hybrid combinations of the profiles in Fig. 5a. We present the average AMF obtained in the sensitivity test using each hybrid profile and its percent difference relative to the mean AMF obtained using the DC3 profile. Because OMI experiences a more limited range of solar zenith angles during summer over the US ($\sim 30^\circ \pm 6^\circ$, on

Table 2. Results of the AMF sensitivity tests on the hybrid profiles in Fig. 5.

Profile	Avg. AMF	% Δ AMF vs. DC3	Avg. AMF SZA < 40°	% Δ AMF (SZA < 40°) vs. DC3
DC3	1.59	–	1.33	–
Free-trop. hybrid-0	1.04	–34.42	0.99	–25.51
Mid-trop. hybrid-0	1.58	–0.80	1.31	–1.02
Free-trop. hybrid-500	1.54	–3.56	1.31	–1.07
Mid-trop. hybrid-500	1.63	2.12	1.36	2.69
Free-trop. hybrid-665	1.64	3.24	1.39	4.37
Mid-trop. hybrid-665	1.64	3.23	1.38	3.98
Free-trop. hybrid-500, nudge	1.29	–19.18	1.15	–13.73
Mid-trop. hybrid-500, nudge	1.59	–0.07	1.33	–0.07
Free-trop. hybrid-500, nudge, 2x flash rate	1.51	–5.52	1.29	–3.13
Mid-trop. hybrid-500, nudge, 2x flash rate	1.61	1.11	1.34	1.26

average) than is defined in the TOMRAD lookup table, we also compare a subset of the AMF sensitivity tests with the SZA < 40°.

Comparing the 0 mol flash^{–1} WRF-Chem profiles to the DC3 profile, we see that the difference in NO₂ above 375 hPa has a large impact on the AMF, causing a 25–35 % low bias in the AMF, depending on the SZAs considered. Adding lightning NO_x to the WRF-Chem simulation (the 500 and 665 mol flash^{–1} profiles) corrects this bias. Recent work (Nault et al., 2017) suggests that the previous mean value of mol NO flash^{–1} (500 mol flash^{–1}) is 33 % lower; comparing the AMFs obtained from profiles generated with 500 and 665 mol flash^{–1} changes the sign of the AMF bias relative to the DC3 profile, but not its magnitude.

The purpose of including the mid-troposphere hybrid profiles, which only use the WRF-Chem profile between 700 and 375 hPa, is to evaluate the impact of the simulated NO₂ maximum around 500 hPa. In almost all cases, the bias of these hybrid profiles against the DC3 profile is less than the corresponding free-troposphere hybrid. Thus, that anomalous maximum at 500 hPa has a smaller impact than the overall presence or absence of lightning NO₂, as one would expect.

An additional complication arises when considering the effect of nudging the model meteorology. By default, the meteorology in WRF is driven by the model's internal physics and is constrained by reanalysis meteorology only through the initial and boundary conditions. WRF has the option, however, to constrain meteorology throughout the domain using four-dimensional data analysis nudging. The temperature and water vapor mixing ratio can both be nudged, and both are used in the Grell 3D cumulus physics calculation in WRF (Grell, 1993; Grell and Dévényi, 2002), which outputs the cloud top height that is used by the Price and Rind (1992) parameterization of flash rate.

With FDDA nudging, lightning flash rates throughout the domain decreased by approximately a factor of 2 compared to the unnudged case (Fig. S3). Comparing both temperature and water vapor mixing ratios from nudged and unnudged

simulations, we find that nudged and unnudged temperature profiles only differ by ~1–2 K at each model level on average, and both agree well with DC3 measurements. The water vapor profiles change more significantly, and the profiles resulting from the nudged simulation agree better with those measured during DC3 (Fig. S4). Therefore, we conclude that the changes to the water vapor profiles are responsible for the 2x change in lightning flash rates.

Using the NO₂ profiles resulting from the nudged simulation with 500 mol flash^{–1}, we see in Fig. 5a that there is significantly less simulated NO₂ near 200 hPa than in the unnudged run and the DC3 observations. The AMF sensitivity tests show that this reintroduces a 14–19 % low bias compared to the AMF derived from the DC3 profile – a significant increase in the bias compared to the unnudged simulation. Doubling the flash rate largely corrects this bias by increasing the NO₂ found in the upper part of the profile (Fig. 5a).

3.3 Effect of varied lightning emissions on BEHR AMFs

To illustrate the impact of missing lightning NO_x on a full retrieval, we use the unnudged WRF-Chem NO₂ profiles simulated with 0, 500, and 665 mol NO flash^{–1} as a priori profiles in the BEHR retrieval and examine the change in both AMF and retrieval NO₂ vertical column density with the change in simulated lightning NO_x.

Figure 6 shows the average percent change in AMFs (top) and absolute change in VCDs (bottom) between retrievals using profiles generated using 0 and 500 mol NO flash^{–1} (Fig. 6a, c) and between 500 and 665 mol NO flash^{–1} (Fig. 6b, d). These results were obtained by averaging data from 18 May to 23 June 2012, treating the data as described in Sect. 2.5.1.

Most importantly, we see in Fig. 6a that the change due to the inclusion of lightning NO₂ is not constant throughout the domain, but is regionally specific. The southeast US sees

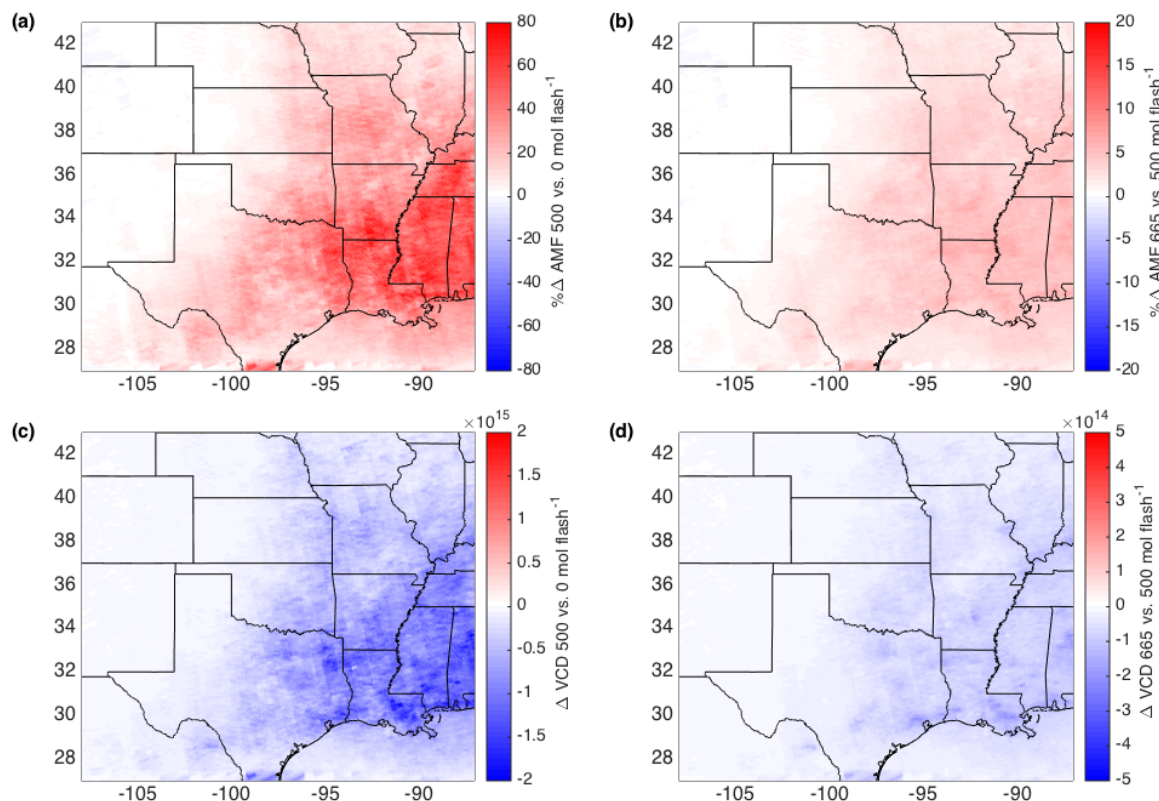


Figure 6. Average percent difference in AMFs (**a**, **b**) and absolute difference in VCDs (**c**, **d**) averaged over the time period 18 May–23 June 2012. (**a**, **c**) Difference between profiles generated using 500 and 0 mol NO flash⁻¹; (**b**, **d**) difference between profiles generated using 665 and 500 mol NO flash⁻¹. Note that in panels (**c**) and (**d**) the color scale is one-fourth that of panels (**a**) and (**b**).

the greatest change in AMF, as it has very active lightning (Hudman et al., 2007). This leads to changes in the retrieved VCD of 1 to 2×10^{15} molec. cm⁻².

We consider two uncertainty values to determine if this change is significant. Bucselo et al. (2013) calculated a global mean uncertainty of 1×10^{15} molec. cm⁻² for tropospheric NO₂ VCDs. Boersma et al. (2004) calculated a typical uncertainty of 23 % in tropospheric AMFs for polluted conditions. Since, on average, 32 ± 6 (mean $\pm 1\sigma$) pixels contribute to each value in our average, the reduced uncertainty is $\sim 0.2 \times 10^{15}$ molec. cm⁻² and 4 %, respectively. The changes we find in the tropospheric VCD due to the inclusion or exclusion of lightning NO₂ from the a priori profiles exceed the uncertainty in ~ 50 % of the domain; the changes in the AMF exceed the uncertainty in ~ 70 % of the domain.

The effect on the retrieval from increasing the mol NO flash⁻¹ from 500 to 665 is about 5–10x smaller, as seen in Fig. 6b, d. In Figs. 1 and 5, we see that the change in the UT profile is smaller when increasing the mol flash⁻¹ from 500 to 665 compared to increasing from 0 to 500 as expected. The nonlinear nature of the AMF calculation also contributes to the smaller change in AMFs and VCDs between 500 and 665 mol flash⁻¹ profiles; as the contribution of lightning NO₂ increases, both the numerator

(at the relevant pressure levels) and denominator of Eq. (3) increase. The increasing denominator will cause the same magnitude increase in the numerator to have a smaller effect on the overall AMF.

4 Discussion

Accurately representing lightning NO₂ in a priori profiles for retrieval of NO₂ from space is vital not only when retrieving lightning events but for any retrieval in a region and time period influenced by lightning. Work from the DC3 campaign has shown that the lifetime of NO_x in the near field of thunderstorms is remarkably short (~ 3 h, Nault et al., 2016) due to active chemistry with peroxy radical species convected from the surface. We note that the WRF-Chem model used here may not be adequately capturing this near-field chemistry as the simulated concentrations of methyl peroxy nitrate are significantly lower than those measured by the DC3 campaign, particularly in the range of 300 to 400 hPa. We suspect that modeled concentrations of the methyl peroxy radical precursor are too low, but we have not investigated this. However, we do not believe this significantly impacts our conclusions, as, when we bin the DC3 MPN data as in

Fig. 5, the MPN concentration is one-fifth to one-tenth that of NO_x , so the effect on the AMF is expected to be less than the effect of increasing the modeled mol NO flash⁻¹ from 500 to 665.

As discussed in Nault et al. (2017), once those peroxy radicals are depleted, the UT lifetime of NO_x in the far field from thunderstorms is in the range of 0.5 to 1.5 days (Nault et al., 2016, 2017). As shown in Sect. 3.1, this means that the presence or absence of lightning NO_2 in the a priori profiles has a large effect on the retrieval AMFs in clear sky conditions which are used to obtain information about boundary layer NO_x (e.g., Lamsal et al., 2010; Beirle et al., 2011; Valin et al., 2013; Lamsal et al., 2015; Lu et al., 2015; Liu et al., 2016, 2017). Since many of these studies focus on summer months when thunderstorms are common over the US (Barth et al., 2015), the inclusion of lightning NO_2 in the a priori profiles is necessary to accurately constrain the emissions. Lightning is less frequent in wintertime, but the southeast US does experience winter lightning (Orville et al., 2001; Hunter et al., 2001). Therefore, wintertime retrievals will likely see significantly less but nonzero impact from the inclusion of lightning NO_2 in the a priori profiles. Future work will verify this as new a priori profiles are planned for inclusion in the next generation of the BEHR retrieval. These new a priori profiles will correct the absence of modeled lightning NO_2 in the BEHR v2.1C a priori profiles.

4.1 Effect of nudged meteorology on flash counts

Although our results showed that the NO_2 profile resulting from the nudged run without doubled flash counts had less UT NO_2 than the average DC3 profile, we cannot conclude that the flash rates calculated with nudged meteorology are underestimated, particularly as Wong et al. (2013) found the opposite result when comparing to the National Lightning Detection Network. A direct comparison with Wong et al. (2013) is complicated by the different choices of model options (such as cumulus physics: Grell 3D in ours vs. Grell-Devenyi in Wong et al., 2013; Lin vs. Thompson microphysics; NARR vs. NCEP Global Forecasting System final meteorology). A full analysis of the reason that activating FDDA nudging causes the flash rates to decrease by 50 % in our case is beyond the scope of this paper. Empirically, we see that the NO_2 profile generated by the FDDA run with 1x the base flash rate has less UT NO_2 than was observed during DC3 (Fig. 5). Therefore, we cannot say whether this discrepancy in the profile is due to the reduced number of flashes or a too-low average number of moles of NO emitted per flash. Our correction of doubling the nudged flash rate to improve agreement between the modeled and observed profiles was the most straightforward based on the differences between the nudged and unnudged runs.

Laughner et al. (2016) showed the importance of using daily, high-spatial-resolution a priori profiles to accurately resolve differences in NO_2 VCDs upwind and downwind of

a city and suggested the use of nudging to reduce the uncertainty due to wind direction, especially. Those results also indicated that using daily, high-spatial-resolution profiles is essential to directly constrain emissions with satellite observations. Our results here indicate that (1) missing lightning NO_2 in the a priori profiles will lead to large overestimations of VCDs, which, among other things, would lead to overestimates of NO_x emissions based on such a retrieval, and (2) that, when using nudging within a WRF-Chem simulation to constrain the meteorology, its effect on lightning flash rates must be checked to ensure it does not inadvertently affect the upper tropospheric NO_2 profile.

4.2 Relevance to cloud slicing

In the context of work using cloud-slicing techniques to derive NO_2 profiles (e.g., Choi et al., 2014), our results suggest that profile shape is a minor contribution to the uncertainty. By using a simulated retrieval with a known NO_2 concentration profile, Choi et al. (2014) estimated a 20–30 % uncertainty in the NO_2 concentration derived from their cloud-slicing approach. Our work here shows that, for fully cloudy conditions, the change in the AMF between a no-lightning and 500 mol flash⁻¹ NO_2 profile is ≤ 5 % (Sect. 3.1). Since Choi et al. (2014) used a typical C-shaped NO_2 profile that included lightning NO_2 (e.g., Pickering et al., 1998), based on our results, we expect that any uncertainty should be closer to the difference we observed between the 500 and 665 mol flash⁻¹ profiles, ≤ 1 %, although we acknowledge that the analysis in Choi et al. (2014) may include additional sources of uncertainty not captured by our work.

4.3 Relevance to global and geostationary retrievals

To the best of our knowledge, the chemical transport models used to generate the a priori profiles in the NASA standard product and KNMI DOMINO product for OMI NO_2 include lightning NO_x in the simulation. However, for researchers wishing to generate high-spatial-resolution a priori profiles using models such as WRF-Chem or the Community Multi-scale Air Quality model that have thus far focused on lower troposphere chemistry for air quality implications, it is important to verify whether that model setup includes lightning NO_x . Retrievals that use a priori profiles without a lightning NO_x parameterization will suffer from a regionally dependent, systematic positive bias in retrieved VCDs. This is particularly difficult to account for given that the bias is unlikely to be reduced by averaging, nor is it constant enough spatially to be addressed as a coarse, ad hoc correction to the AMF.

The next generation of polar-orbiting (TROPOMI) and geostationary (TEMPO, Sentinel-5, GEMS) UV-visible spectrometers will have even greater spatial resolution than OMI. To get the most value out of these high-spatial-resolution detectors, high-spatial-resolution and temporal-

resolution a priori profiles are necessary (e.g., Russell et al., 2011; Laughner et al., 2016; Goldberg et al., 2017). High-resolution air quality models, such as WRF-Chem or CMAQ, are one avenue to produce a priori profiles with a resolution of 1 to 10 km. Ensuring that lightning NO_x is adequately parameterized in the models is essential for any retrieval, but especially for geostationary satellites such as TEMPO, which will retrieve NO_2 at larger solar zenith angles than polar-orbiting satellites. At such large SZAs, the relative importance of accurate UT NO_2 profiles is even greater than for OMI retrievals.

5 Conclusions

We quantify the impact of lightning NO_2 on a priori profiles used in satellite retrievals of NO_2 . We find that, on average, compared to an average NO_2 profile constructed from measurements taken during the DC3 campaign, excluding lightning NO_2 leads to a -35% bias in the AMF if all solar zenith angles are considered, and -25% for solar zenith angles relevant to the OMI instrument in the summer. We find that, using the Price and Rind (1992) parameterization in WRF-Chem with the Grell-3D cumulus model, 500 to 665 mol NO flash $^{-1}$ yields AMFs within $\sim 5\%$ of those obtained using the DC3 profile. We also find that, if FDDA nudging is used, flash rates must be multiplied by a factor of 2 to get the same agreement with this model configuration.

Implementing profiles generated with 0, 500, and 665 mol NO flash $^{-1}$ in the BEHR retrieval, we find that the effect on the AMF is very regionally dependent. For summertime retrievals, changing from profiles using 0 to 500 mol NO flash $^{-1}$ shows the largest increase in the AMF of 50–80% occurring in the southeast US. This results in changes to the VCD of 1 to 2×10^{15} molec. cm $^{-2}$. The effect is nearly 0 on the west edge of the domain, over the Rocky Mountains. Further increasing the mol NO flash $^{-1}$ from 500 to 665 only results in a $\sim 5\%$ change to the AMF.

Code and data availability. The AutoWRFChem code used to automate the preparation of meteorological and chemical inputs and execution of WRF-Chem is available at <https://github.com/CohenBerkeleyLab/AutoWRFChem-Base> (Laughner, 2017b). The versions of WRF-Chem v3.5.1, WPS v3.5.1, NEI conversion utility, MEGAN biogenic model, and MOZBC utility with the modification to handle the R2SMH chemical mechanism and corresponding emissions are available at <https://github.com/CohenBerkeleyLab/AutoWRFChem-R2SMH>, v1.0.0. The retrievals used in Sect. 3.3 are available at <https://doi.org/10.6078/D19S9D> (Laughner and Cohen, 2017). The analysis code, TOMRAD LUT, and WRF-Chem name-list files are available at <https://doi.org/10.5281/zenodo.1001803> (Laughner, 2017a). For access to the BEHR algorithm contact the corresponding author, R. C. Cohen.

The version 2.1 NASA Aura OMI NO_2 standard product was obtained from the Goddard Earth Sciences Data and Information

Services Center (GES DISC) in Greenbelt, MD, USA (Krotkov and Veefkind, 2016). The MODIS Aqua Clouds 5-Min L2 Swath 1 and 5 km (MYD06_L2; Platnick et al., 2015) and MODIS Terra+Aqua Albedo 16-Day L3 Global 0.05Deg CMG V005 (Schaaf and Wang, 2015) were acquired from the Level-1 and Atmospheric Archive and Distribution System (LAADS) Distributed Active Archive Center (DAAC), located in the Goddard Space Flight Center in Greenbelt, Maryland (<https://ladsweb.nascom.nasa.gov/>).

The Supplement related to this article is available online at <https://doi.org/10.5194/amt-10-4403-2017-supplement>.

Competing interests. The authors declare that they have no conflict of interest.

Acknowledgements. The authors gratefully acknowledge support from the NASA ESS Fellowship NNX14AK89H, NASA grant NNX15AE37G, and the TEMPO project grant SV3-83019. We acknowledge use of the WRF-Chem preprocessor tools MOZBC, fire_emiss, etc. provided by the Atmospheric Chemistry Observations and Modeling (ACOM) laboratory of NCAR. This research used the Savio computational cluster resource provided by the Berkeley Research Computing program at the University of California, Berkeley (supported by the UC Berkeley Chancellor, Vice Chancellor of Research, and Office of the CIO). The authors also wish to thank Mary Barth for assistance with the lightning NO_x module in WRF-Chem.

Edited by: Helen Worden

Reviewed by: two anonymous referees

References

- Acarreta, J. R., De Haan, J. F., and Stammes, P.: Cloud pressure retrieval using the O₂-O₂ absorption band at 477 nm, *J. Geophys. Res.-Atmos.*, 109, D05204, <https://doi.org/10.1029/2003JD003915>, 2004.
- Allen, D. J., Pickering, K. E., Pinder, R. W., Henderson, B. H., Appel, K. W., and Prados, A.: Impact of lightning-NO on eastern United States photochemistry during the summer of 2006 as determined using the CMAQ model, *Atmos. Chem. Phys.*, 12, 1737–1758, <https://doi.org/10.5194/acp-12-1737-2012>, 2012.
- Apel, E. C., Olson, J. R., Crawford, J. H., Hornbrook, R. S., Hills, A. J., Cantrell, C. A., Emmons, L. K., Knapp, D. J., Hall, S., Mauldin III, R. L., Weinheimer, A. J., Fried, A., Blake, D. R., Crouse, J. D., Clair, J. M. St., Wennberg, P. O., Diskin, G. S., Fuelberg, H. E., Wisthaler, A., Mikoviny, T., Brune, W., and Riemer, D. D.: Impact of the deep convection of isoprene and other reactive trace species on radicals and ozone in the upper troposphere, *Atmos. Chem. Phys.*, 12, 1135–1150, <https://doi.org/10.5194/acp-12-1135-2012>, 2012.

- Barth, M. C., Cantrell, C. A., Brune, W. H., Rutledge, S. A., Crawford, J. H., Huntrieser, H., Carey, L. D., MacGorman, D., Weisman, M., Pickering, K. E., Bruning, E., Anderson, B., Apel, E., Biggerstaff, M., Campos, T., Campuzano-Jost, P., Cohen, R., Crouse, J., Day, D. A., Diskin, G., Flocke, F., Fried, A., Garland, C., Heikes, B., Honomichl, S., Hornbrook, R., Huey, L. G., Jimenez, J. L., Lang, T., Lichtenstern, M., Mikoviny, T., Nault, B., O'Sullivan, D., Pan, L. L., Peischl, J., Pollack, I., Richter, D., Riener, D., Ryerson, T., Schlager, H., Clair, J. S., Walega, J., Weibring, P., Weinheimer, A., Wennberg, P., Wisthaler, A., Wooldridge, P. J., and Ziegler, C.: The Deep Convective Clouds and Chemistry (DC3) Field Campaign, *B. Am. Meteorol. Soc.*, 96, 1281–1309, <https://doi.org/10.1175/bams-d-13-00290.1>, 2015.
- Beirle, S., Salzmann, M., Lawrence, M. G., and Wagner, T.: Sensitivity of satellite observations for freshly produced lightning NO_x , *Atmos. Chem. Phys.*, 9, 1077–1094, <https://doi.org/10.5194/acp-9-1077-2009>, 2009.
- Beirle, S., Boersma, K., Platt, U., Lawrence, M., and Wagner, T.: Megacity Emissions and Lifetimes of Nitrogen Oxides Probed from Space, *Science*, 333, 1737–1739, 2011.
- Bertram, T. H., Perring, A. E., Wooldridge, P. J., Crouse, J. D., Kwan, A. J., Wennberg, P. O., Scheuer, E., Dibb, J., Avery, M., Sachse, G., Vay, S. A., Crawford, J. H., McNaughton, C. S., Clarke, A., Pickering, K. E., Fuelberg, H., Huey, G., Blake, D. R., Singh, H. B., Hall, S. R., Shetter, R. E., Fried, A., Heikes, B. G., and Cohen, R. C.: Direct Measurements of the Convective Recycling of the Upper Troposphere, *Science*, 315, 816–820, <https://doi.org/10.1126/science.1134548>, 2007.
- Boccippio, D., Cummins, K., Christian, H., and Goodman, S.: Combined Satellite- and Surface-Based Estimation of the Intracloud-Cloud-to-Ground Lightning Ratio over the Continental United States, *Mon. Weather Rev.*, 129, 108–122, 2001.
- Boersma, K., Bucsel, E., Brinksma, E., and Gleason, J.: NO_2 , in: OMI Algorithm Theoretical Basis Document, vol. 4, OMI Trace Gas Algorithms, ATB-OMI-04, version 2.0, 13–36, available at: <http://eosps.nasa.gov/sites/default/files/atbd/ATBD-OMI-04.pdf> (last access: 13 November 2017), 2002.
- Boersma, K., Eskes, H., and Brinksma, E.: Error analysis for tropospheric NO_2 retrieval from space, *J. Geophys. Res.-Atmos.*, 106, D04311, <https://doi.org/10.1029/2003JD003962>, 2004.
- Boersma, K. F., Eskes, H. J., Dirksen, R. J., van der A, R. J., Veefkind, J. P., Stammes, P., Huijnen, V., Kleipool, Q. L., Sneep, M., Claas, J., Leitão, J., Richter, A., Zhou, Y., and Brunner, D.: An improved tropospheric NO_2 column retrieval algorithm for the Ozone Monitoring Instrument, *Atmos. Meas. Tech.*, 4, 1905–1928, <https://doi.org/10.5194/amt-4-1905-2011>, 2011.
- Browne, E. C., Perring, A. E., Wooldridge, P. J., Apel, E., Hall, S. R., Huey, L. G., Mao, J., Spencer, K. M., Clair, J. M. St., Weinheimer, A. J., Wisthaler, A., and Cohen, R. C.: Global and regional effects of the photochemistry of $\text{CH}_3\text{O}_2\text{NO}_2$: evidence from ARCTAS, *Atmos. Chem. Phys.*, 11, 4209–4219, <https://doi.org/10.5194/acp-11-4209-2011>, 2011.
- Browne, E. C., Wooldridge, P. J., Min, K.-E., and Cohen, R. C.: On the role of monoterpene chemistry in the remote continental boundary layer, *Atmos. Chem. Phys.*, 14, 1225–1238, <https://doi.org/10.5194/acp-14-1225-2014>, 2014.
- Bucsel, E. J., Celarier, E. A., Wenig, M. O., Gleason, J. F., Veefkind, J. P., Boersma, K. F., and Brinksma, E. J.: Algorithm for NO_2 vertical column retrieval from the ozone monitoring instrument, *IEEE T. Geosci. Remote*, 44, 1245–1258, <https://doi.org/10.1109/TGRS.2005.863715>, 2006.
- Bucsel, E. J., Krotkov, N. A., Celarier, E. A., Lamsal, L. N., Swartz, W. H., Bhartia, P. K., Boersma, K. F., Veefkind, J. P., Gleason, J. F., and Pickering, K. E.: A new stratospheric and tropospheric NO_2 retrieval algorithm for nadir-viewing satellite instruments: applications to OMI, *Atmos. Meas. Tech.*, 6, 2607–2626, <https://doi.org/10.5194/amt-6-2607-2013>, 2013.
- Choi, S., Joiner, J., Choi, Y., Duncan, B. N., Vasilkov, A., Krotkov, N., and Bucsel, E.: First estimates of global free-tropospheric NO_2 abundances derived using a cloud-slicing technique applied to satellite observations from the Aura Ozone Monitoring Instrument (OMI), *Atmos. Chem. Phys.*, 14, 10565–10588, <https://doi.org/10.5194/acp-14-10565-2014>, 2014.
- Cooray, V., Rahman, M., and Rakov, V.: On the NO_x production by laboratory electrical discharges and lightning, *J. Atmos. Sol.-Terr. Phys.*, 71, 1877–1889, <https://doi.org/10.1016/j.jastp.2009.07.009>, 2009.
- Emmons, L. K., Walters, S., Hess, P. G., Lamarque, J.-F., Pfister, G. G., Fillmore, D., Granier, C., Guenther, A., Kinnison, D., Laepple, T., Orlando, J., Tie, X., Tyndall, G., Wiedinmyer, C., Baughcum, S. L., and Kloster, S.: Description and evaluation of the Model for Ozone and Related chemical Tracers, version 4 (MOZART-4), *Geosci. Model Dev.*, 3, 43–67, <https://doi.org/10.5194/gmd-3-43-2010>, 2010.
- EPA: Air Pollutant Emissions Trends Data, available at: <https://www.epa.gov/air-emissions-inventories/air-pollutant-emissions-trends-data>, last access: 11 October 2016.
- Goldberg, D. L., Lamsal, L. N., Loughner, C. P., Swartz, W. H., Lu, Z., and Streets, D. G.: A high-resolution and observationally constrained OMI NO_2 satellite retrieval, *Atmos. Chem. Phys.*, 17, 11403–11421, <https://doi.org/10.5194/acp-17-11403-2017>, 2017.
- Goliff, W. S., Stockwell, W. R., and Lawson, C. V.: The regional atmospheric chemistry mechanism, version 2, *Atmos. Environ.*, 68, 174–185, <https://doi.org/10.1016/j.atmosenv.2012.11.038>, 2013.
- Grell, G. A.: Prognostic Evaluation of Assumptions Used by Cumulus Parameterizations, *Mon. Weather Rev.*, 121, 764–787, [https://doi.org/10.1175/1520-0493\(1993\)121<0764:PEOAUB>2.0.CO;2](https://doi.org/10.1175/1520-0493(1993)121<0764:PEOAUB>2.0.CO;2), 1993.
- Grell, G. A. and Dévényi, D.: A generalized approach to parameterizing convection combining ensemble and data assimilation techniques, *Geophys. Res. Lett.*, 29, 38–1–38–4, <https://doi.org/10.1029/2002gl015311>, 2002.
- Grell, G. A., Peckham, S. E., Schmitz, R., McKeen, S. A., Frost, G., Skamarock, W. C., and Eder, B.: Fully coupled “online” chemistry within the WRF model, *Atmos. Environ.*, 39, 6957–6975, <https://doi.org/10.1016/j.atmosenv.2005.04.027>, 2005.
- Guenther, A., Karl, T., Harley, P., Wiedinmyer, C., Palmer, P. I., and Geron, C.: Estimates of global terrestrial isoprene emissions using MEGAN (Model of Emissions of Gases and Aerosols from Nature), *Atmos. Chem. Phys.*, 6, 3181–3210, <https://doi.org/10.5194/acp-6-3181-2006>, 2006.
- Hastings, D. and Dunbar, P.: Global Land One-kilometer Base Elevation (GLOBE) Digital Elevation Model, Documentation, Volume 1.0. National Oceanic and Atmospheric Administration, Na-

- tional Geophysical Data Center, 325 Broadway, Boulder, Colorado 80303, USA, 1999.
- Hönninger, G., von Friedeburg, C., and Platt, U.: Multi axis differential optical absorption spectroscopy (MAX-DOAS), *Atmos. Chem. Phys.*, 4, 231–254, <https://doi.org/10.5194/acp-4-231-2004>, 2004.
- Hudman, R. C., Jacob, D. J., Turquety, S., Leibensperger, E. M., Murray, L. T., Wu, S., Gilliland, A. B., Avery, M., Bertram, T. H., Brune, W., Cohen, R. C., Dibb, J. E., Flocke, F. M., Fried, A., Holloway, J., Neuman, J. A., Orville, R., Perring, A., Ren, X., Sachse, G. W., Singh, H. B., Swanson, A., and Wooldridge, P. J.: Surface and lightning sources of nitrogen oxides over the United States: Magnitudes, chemical evolution, and outflow, *J. Geophys. Res.-Atmos.*, 112, D12S05, <https://doi.org/10.1029/2006JD007912>, 2007.
- Hudman, R. C., Moore, N. E., Mebust, A. K., Martin, R. V., Russell, A. R., Valin, L. C., and Cohen, R. C.: Steps towards a mechanistic model of global soil nitric oxide emissions: implementation and space based-constraints, *Atmos. Chem. Phys.*, 12, 7779–7795, <https://doi.org/10.5194/acp-12-7779-2012>, 2012.
- Hudson, R., Kim, J.-H., and Anne, M. T.: On the derivation of tropospheric column ozone from radiances measured by the total ozone mapping spectrometer, *J. Geophys. Res.-Atmos.*, 100, 11134–11145, 1995.
- Hunter, S. M., Underwood, S. J., Holle, R. L., and Mote, T. L.: Winter Lightning and Heavy Frozen Precipitation in the Southeast United States, *Weather Forecast.*, 16, 478–490, [https://doi.org/10.1175/1520-0434\(2001\)016<0478:wlahfp>2.0.co;2](https://doi.org/10.1175/1520-0434(2001)016<0478:wlahfp>2.0.co;2), 2001.
- Jaeglé, L., Jacob, D. J., Wang, Y., Weinheimer, A. J., Ridley, B. A., Campos, T. L., Sachse, G. W., and Hagen, D. E.: Sources and chemistry of NO_x in the upper troposphere over the United States, *Geophys. Res. Lett.*, 25, 1705–1708, <https://doi.org/10.1029/97GL03591>, 1998.
- Krotkov, N. A. and Veefkind, P.: OMI/Aura Nitrogen Dioxide (NO₂) Total and Tropospheric Column 1-orbit L2 Swath 13 × 24 km V003, version 003, Greenbelt, MD, USA, Goddard Earth Sciences Data and Information Services Center (GES DISC), <https://doi.org/10.5067/Aura/OMI/DATA2017>, 2016.
- Krotkov, N. A., Lamsal, L. N., Celarier, E. A., Swartz, W. H., Marchenko, S. V., Bucsela, E. J., Chan, K. L., Wenig, M., and Zara, M.: The version 3 OMI NO₂ standard product, *Atmos. Meas. Tech.*, 10, 3133–3149, <https://doi.org/10.5194/amt-10-3133-2017>, 2017.
- Kuhlmann, G., Lam, Y. F., Cheung, H. M., Hartl, A., Fung, J. C. H., Chan, P. W., and Wenig, M. O.: Development of a custom OMI NO₂ data product for evaluating biases in a regional chemistry transport model, *Atmos. Chem. Phys.*, 15, 5627–5644, <https://doi.org/10.5194/acp-15-5627-2015>, 2015.
- Lamsal, L. N., Martin, R. V., van Donkelaar, A., Celarier, E. A., Bucsela, E. J., Boersma, K. F., Dirksen, R., Luo, C., and Wang, Y.: Indirect validation of tropospheric nitrogen dioxide retrieved from the OMI satellite instrument: Insight into the seasonal variation of nitrogen oxides at northern midlatitudes, *J. Geophys. Res.-Atmos.*, 115, D05302, <https://doi.org/10.1029/2009JD013351>, 2010.
- Lamsal, L. N., Duncan, B. N., Yoshida, Y., Krotkov, N. A., Pickering, K. E., Streets, D. G., and Lu, Z.: U.S. NO₂ trends (2005–2013): EPA Air Quality System (AQS) data versus improved observations from the Ozone Monitoring Instrument (OMI), *Atmos. Environ.*, 110, 130–143, <https://doi.org/10.1016/j.atmosenv.2015.03.055>, 2015.
- Laughner, J. L.: Analysis code and intermediate data for “Quantification of the effect of modeled lightning NO₂ on UV-visible air mass factors”, <https://doi.org/10.5281/zenodo.1001803>, 2017a.
- Laughner, J. L.: AutoWRFChem-Base v0.1.0: Automation for the WRF-Chem model, <https://doi.org/10.5281/zenodo.834798>, 2017b.
- Laughner, J. L. and Cohen, R. C.: Demonstration retrievals from “Quantification of the effect of modeled lightning NO₂ on UV-visible air mass factors”, v2, UC Berkeley Dash, Dataset, <https://doi.org/10.6078/D19S9D>, 2017.
- Laughner, J. L., Zare, A., and Cohen, R. C.: Effects of daily meteorology on the interpretation of space-based remote sensing of NO₂, *Atmos. Chem. Phys.*, 16, 15247–15264, <https://doi.org/10.5194/acp-16-15247-2016>, 2016.
- Levelt, P., van der Oord, G., Dobber, M., Mälkki, A., Visser, H., de Vries, J., Stammes, P., Lundell, J., and Saari, H.: The Ozone Monitoring Instrument, *IEEE T. Geosci. Remote*, 44, 1093–1101, <https://doi.org/10.1109/TGRS.2006.872333>, 2006.
- Lin, J.-T., Liu, M.-Y., Xin, J.-Y., Boersma, K. F., Spurr, R., Martin, R., and Zhang, Q.: Influence of aerosols and surface reflectance on satellite NO₂ retrieval: seasonal and spatial characteristics and implications for NO_x emission constraints, *Atmos. Chem. Phys.*, 15, 11217–11241, <https://doi.org/10.5194/acp-15-11217-2015>, 2015.
- Lin, Y.-L., Farley, R. D., and Orville, H. D.: Bulk Parameterization of the Snow Field in a Cloud Model, *J. Clim. Appl. Meteorol.*, 22, 1065–1092, 1983.
- Liu, F., Beirle, S., Zhang, Q., Dörner, S., He, K., and Wagner, T.: NO_x lifetimes and emissions of cities and power plants in polluted background estimated by satellite observations, *Atmos. Chem. Phys.*, 16, 5283–5298, <https://doi.org/10.5194/acp-16-5283-2016>, 2016.
- Liu, F., Beirle, S., Zhang, Q., van der A, R. J., Zheng, B., Tong, D., and He, K.: NO_x emission trends over Chinese cities estimated from OMI observations during 2005 to 2015, *Atmos. Chem. Phys.*, 17, 9261–9275, <https://doi.org/10.5194/acp-17-9261-2017>, 2017.
- Liu, Y., Bourgeois, A., Warner, T., Swerdlin, S., and Hacker, J.: Implementation of the observation-nudging based on FDDA into WRF for supporting AFEC test operations, 6th WRF Conference, NCAR, 27–30 June 2005, Boulder, CO, USA, 10.7, 2005.
- Lu, Z., Streets, D. G., de Foy, B., Lamsal, L. N., Duncan, B. N., and Xing, J.: Emissions of nitrogen oxides from US urban areas: estimation from Ozone Monitoring Instrument retrievals for 2005–2014, *Atmos. Chem. Phys.*, 15, 10367–10383, <https://doi.org/10.5194/acp-15-10367-2015>, 2015.
- Martin, R., Sauvage, B., Folkins, I., Sioris, C., Boone, C., Bernath, P., and Ziemke, J.: Space-based constraints on the production of nitric oxide by lightning, *J. Geophys. Res.-Atmos.*, 112, D09309, <https://doi.org/10.1029/2006JD007831>, 2007.
- McLinden, C. A., Fioletov, V., Boersma, K. F., Kharol, S. K., Krotkov, N., Lamsal, L., Makar, P. A., Martin, R. V., Veefkind, J. P., and Yang, K.: Improved satellite retrievals of NO₂ and SO₂ over the Canadian oil sands and comparisons with surface measurements, *Atmos. Chem. Phys.*, 14, 3637–3656, <https://doi.org/10.5194/acp-14-3637-2014>, 2014.

- Mebust, A. and Cohen, R.: Observations of a seasonal cycle in NO_x emissions from fires in African woody savannas, *Geophys. Res. Lett.*, 40, 1451–1455, <https://doi.org/10.1002/grl.50343>, 2013.
- Mebust, A. K. and Cohen, R. C.: Space-based observations of fire NO_x emission coefficients: a global biome-scale comparison, *Atmos. Chem. Phys.*, 14, 2509–2524, <https://doi.org/10.5194/acp-14-2509-2014>, 2014.
- Mebust, A. K., Russell, A. R., Hudman, R. C., Valin, L. C., and Cohen, R. C.: Characterization of wildfire NO_x emissions using MODIS fire radiative power and OMI tropospheric NO₂ columns, *Atmos. Chem. Phys.*, 11, 5839–5851, <https://doi.org/10.5194/acp-11-5839-2011>, 2011.
- Miyazaki, K., Eskes, H. J., and Sudo, K.: Global NO_x emission estimates derived from an assimilation of OMI tropospheric NO₂ columns, *Atmos. Chem. Phys.*, 12, 2263–2288, <https://doi.org/10.5194/acp-12-2263-2012>, 2012.
- Miyazaki, K., Eskes, H. J., Sudo, K., and Zhang, C.: Global lightning NO_x production estimated by an assimilation of multiple satellite data sets, *Atmos. Chem. Phys.*, 14, 3277–3305, <https://doi.org/10.5194/acp-14-3277-2014>, 2014.
- Nault, B. A., Garland, C., Pusede, S. E., Wooldridge, P. J., Ullmann, K., Hall, S. R., and Cohen, R. C.: Measurements of CH₃O₂NO₂ in the upper troposphere, *Atmos. Meas. Tech.*, 8, 987–997, <https://doi.org/10.5194/amt-8-987-2015>, 2015.
- Nault, B. A., Garland, C., Wooldridge, P. J., Brune, W. H., Campuzano-Jost, P., Crouse, J. D., Day, D. A., Dibb, J., Hall, S. R., Huey, L. G., Jimenez, J. L., Liu, X., Mao, J., Mikoviny, T., Peischl, J., Pollack, I. B., Ren, X., Ryerson, T. B., Scheuer, E., Ullmann, K., Wennberg, P. O., Wisthaler, A., Zhang, L., and Cohen, R. C.: Observational Constraints on the Oxidation of NO_x in the Upper Troposphere, *J. Phys. Chem. A*, 120, 1468–1478, <https://doi.org/10.1021/acs.jpca.5b07824>, 2016.
- Nault, B. A., Laughner, J. L., Wooldridge, P. J., Crouse, J. D., Dibb, J., Diskin, G., Peischl, J., Podolske, J. R., Pollack, I. B., Ryerson, T. B., Scheuer, E., Wennberg, P. O., and Cohen, R. C.: Lightning NO_x Emissions: Reconciling Measured and Modeled Estimates With Updated NO_x Chemistry, *Geophys. Res. Lett.*, 44, 9479–9488, <https://doi.org/10.1002/2017GL074436>, 2017.
- Orville, R. E., Huffines, G., Nielsen-Gammon, J., Zhang, R., Ely, B., Steiger, S., Phillips, S., Allen, S., and Read, W.: Enhancement of cloud-to-ground lightning over Houston, Texas, *Geophys. Res. Lett.*, 28, 2597–2600, <https://doi.org/10.1029/2001GL012990>, 2001.
- Ott, L. E., Pickering, K. E., Stenchikov, G. L., Allen, D. J., DeCaria, A. J., Ridley, B., Lin, R.-F., Lang, S., and Tao, W.-K.: Production of lightning NO_x and its vertical distribution calculated from three-dimensional cloud-scale chemical transport model simulations, *J. Geophys. Res.*, 115, D04301, <https://doi.org/10.1029/2009jd011880>, 2010.
- Palmer, P., Jacob, D., Chance, K., Martin, R., Spurr, R., Kurosu, T., Bey, I., Yantosca, R., Fiore, A., and Li, Q.: Air mass factor formulation for spectroscopic measurements from satellites: Applications to formaldehyde retrievals from the Global Ozone Monitoring Experiment, *J. Geophys. Res.-Atmos.*, 106, 14539–14550, 2001.
- Pickering, K. E., Wang, Y., Tao, W.-K., Price, C., and Müller, J.-F.: Vertical distributions of lightning NO_x for use in regional and global chemical transport models, *J. Geophys. Res.*, 103, 31203–31216, 1998.
- Pickering, K. E., Bucsel, E., Allen, D., Ring, A., Holzworth, R., and Krotkov, N.: Estimates of lightning NO_x production based on OMI NO₂ observations over the Gulf of Mexico, *J. Geophys. Res.-Atmos.*, 121, 8668–8691, <https://doi.org/10.1002/2015JD024179>, 2016.
- Platnick, S., King, M., Wind, G., Ackerman, S., Menzel, P., and Frey, R.: MODIS/Aqua Clouds 5-Min L2 Swath 1 km and 5 km, NASA MODIS Adaptive Processing System, Goddard Space Flight Center, USA, https://doi.org/10.5067/MODIS/MYD06_L2.006, 2015.
- Price, C. and Rind, D.: A simple lightning parameterization for calculating global lightning distributions, *J. Geophys. Res.-Atmos.*, 97, 9919–9933, <https://doi.org/10.1029/92JD00719>, 1992.
- Richter, A. and Wagner, T.: The Use of UV, Visible and Near IR Solar Back Scattered Radiation to Determine Trace Gases, in: *The Remote Sensing of Tropospheric Composition from Space*, edited by: Burrows, J., Platt, U., and Borrell, P., Springer, New York, USA, 2011.
- Russell, A. R., Perring, A. E., Valin, L. C., Bucsel, E. J., Browne, E. C., Wooldridge, P. J., and Cohen, R. C.: A high spatial resolution retrieval of NO₂ column densities from OMI: method and evaluation, *Atmos. Chem. Phys.*, 11, 8543–8554, <https://doi.org/10.5194/acp-11-8543-2011>, 2011.
- Russell, A. R., Valin, L. C., and Cohen, R. C.: Trends in OMI NO₂ observations over the United States: effects of emission control technology and the economic recession, *Atmos. Chem. Phys.*, 12, 12197–12209, <https://doi.org/10.5194/acp-12-12197-2012>, 2012.
- Schaaf, C. and Wang, Z.: MCD43C3 MODIS/Terra+Aqua BRDF/Albedo Albedo Daily L3 Global 0.05Deg CMG V006, NASA EOSDIS Land Processes DAAC, <https://doi.org/10.5067/MODIS/MCD43C3.006>, 2015.
- Schumann, U. and Huntrieser, H.: The global lightning-induced nitrogen oxides source, *Atmos. Chem. Phys.*, 7, 3823–3907, <https://doi.org/10.5194/acp-7-3823-2007>, 2007.
- Schwantes, R. H., Teng, A. P., Nguyen, T. B., Coggon, M. M., Crouse, J. D., St. Clair, J. M., Zhang, X., Schilling, K. A., Seinfeld, J. H., and Wennberg, P. O.: Isoprene NO₃ Oxidation Products from the RO₂ + HO₂ Pathway, *J. Phys. Chem. A*, 119, 10158–10171, <https://doi.org/10.1021/acs.jpca.5b06355>, 2015.
- Seltzer, K. M., Vizuete, W., and Henderson, B. H.: Evaluation of updated nitric acid chemistry on ozone precursors and radiative effects, *Atmos. Chem. Phys.*, 15, 5973–5986, <https://doi.org/10.5194/acp-15-5973-2015>, 2015.
- Sneep, M., de Haan, J. F., Stammes, P., Wang, P., Vanbaue, C., Joiner, J., Vasilkov, A. P., and Levelt, P. F.: Three-way comparison between OMI and PARASOL cloud pressure products, *J. Geophys. Res.-Atmos.*, 113, D15S23, <https://doi.org/10.1029/2007JD008694>, 2008.
- Stammes, P., Sneep, M., de Haan, J. F., Veefkind, J. P., Wang, P., and Levelt, P. F.: Effective cloud fractions from the Ozone Monitoring Instrument: Theoretical framework and validation, *J. Geophys. Res.-Atmos.*, 113, D16S38, <https://doi.org/10.1029/2007JD008820>, 2008.
- Stauffer, D. R. and Seaman, N. L.: Use of four-dimensional data assimilation in a limited-area mesoscale model. Part I: Experiments with synoptic-scale data, *Mon. Weather Rev.*, 118, 1250–1277, 1990.

- Stauffer, D. R., Seaman, N. L., and Binkowski, F. S.: Use of four-dimensional data assimilation in a limited-area mesoscale model. Part II: Effects of data assimilation within the planetary boundary layer, *Mon. Weather Rev.*, 119, 734–754, 1991.
- Thornton, J. A., Wooldridge, P. J., and Cohen, R. C.: Atmospheric NO₂: In Situ Laser-Induced Fluorescence Detection at Parts per Trillion Mixing Ratios, *Anal. Chem.*, 72, 528–539, <https://doi.org/10.1021/ac9908905>, 2000.
- Travis, K. R., Jacob, D. J., Fisher, J. A., Kim, P. S., Marais, E. A., Zhu, L., Yu, K., Miller, C. C., Yantosca, R. M., Sulprizio, M. P., Thompson, A. M., Wennberg, P. O., Crouse, J. D., St. Clair, J. M., Cohen, R. C., Laughner, J. L., Dibb, J. E., Hall, S. R., Ullmann, K., Wolfe, G. M., Pollack, I. B., Peischl, J., Neuman, J. A., and Zhou, X.: Why do models overestimate surface ozone in the Southeast United States?, *Atmos. Chem. Phys.*, 16, 13561–13577, <https://doi.org/10.5194/acp-16-13561-2016>, 2016.
- Valin, L., Russell, A., and Cohen, R.: Variations of OH radical in an urban plume inferred from NO₂ column measurements, *Geophys. Res. Lett.*, 40, 1856–1860, <https://doi.org/10.1002/grl.50267>, 2013.
- Vinken, G. C. M., Boersma, K. F., van Donkelaar, A., and Zhang, L.: Constraints on ship NO_x emissions in Europe using GEOS-Chem and OMI satellite NO₂ observations, *Atmos. Chem. Phys.*, 14, 1353–1369, <https://doi.org/10.5194/acp-14-1353-2014>, 2014.
- Wong, J., Barth, M. C., and Noone, D.: Evaluating a lightning parameterization based on cloud-top height for mesoscale numerical model simulations, *Geosci. Model Dev.*, 6, 429–443, <https://doi.org/10.5194/gmd-6-429-2013>, 2013.
- Zörner, J., Penning de Vries, M., Beirle, S., Sihler, H., Veres, P. R., Williams, J., and Wagner, T.: Multi-satellite sensor study on precipitation-induced emission pulses of NO_x from soils in semi-arid ecosystems, *Atmos. Chem. Phys.*, 16, 9457–9487, <https://doi.org/10.5194/acp-16-9457-2016>, 2016.